Mon. Not. R. Astron. Soc. **000**, 1–21 (2021) Printed 9 November 2023 (MN LATEX style file v2.2)

Cosmic shear beyond 2-point statistics: marginalisation over galaxy intrinsic alignment

Joachim Harnois-Déraps[1]⋆ and others
[1]*School of Mathematics, Statistics and Physics, Newcastle University, Herschel Building, NE1 7RU, Newcastle-upon-Tyne, UK*

Accepted XXX. Received YYY; in original form ZZZ

ABSTRACT
TBD

Key words: Gravitational lensing: weak – Methods: numerical – Cosmology: dark matter, dark energy & large-scale structure of Universe

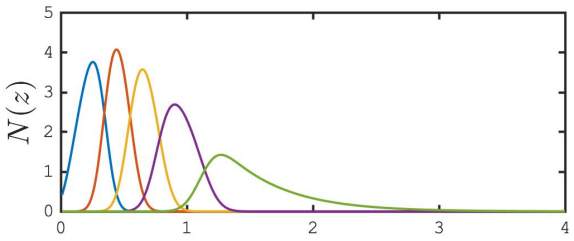

Figure 1. Redshift distribution in our simulations, taken from the Year-1 specifications of the LSST Science Requirement Document (The LSST Dark Energy Science Collaboration et al. 2018) [*check Y1 vs Y10*].

1 INTRODUCTION

Cosmology, gravitational lensing, cosmic shear, 2pt, beyond-2pt, simulations for signal and for secondary signal/systematics, IA-infusion, this paper...

2 COSMIC SHEAR

Cosmic shear can be measured with γ-2PCF or with alternative probes....

2.1 γ-2PCF

Shear two-point correlation functions (γ-2PCFs hereafter) can be predicted with percent-level precision and are therefore an ideal quantity to validate weak lensing simulations. In the Limber approximation[1], the lensing power spectrum C_ℓ^{ij} is obtained from an integral over the three-dimensional matter power spectrum $P_\delta(k,z)$:

$$C_\ell^{ij} = \int_0^{\chi_{\rm H}} \frac{q^i(\chi)\,q^j(\chi)}{\chi^2}\,P_\delta\left(\frac{\ell+1/2}{\chi}, z(\chi)\right)\mathrm{d}\chi, \qquad (1)$$

where $\chi_{\rm H}$ is the co-moving distance to the horizon, c is the speed of light, H_0 the Hubble parameter, and the lensing kernels q^i are given by:

$$q^i(\chi) = \frac{3}{2}\Omega_{\rm m}\left(\frac{H_0}{c}\right)^2\frac{\chi}{a(\chi)}\int_\chi^{\chi_{\rm H}} n^i(\chi')\frac{\mathrm{d}z}{\mathrm{d}\chi'}\frac{\chi'-\chi}{\chi'}\mathrm{d}\chi'\,. \qquad (2)$$

In the previous expression, $n^i(z)$ refers to the redshift distribution in tomographic bin 'i', while $a(\chi)$ is the scale factor at comoving distance χ from the observer [*might need to define Ω_m here]*. The matter power spectrum is computed from Halofit (Takahashi et al. 2012), however other public tools provide $P_\delta(k,z)$ predictions, including e.g. HMcode (Mead et al. 2020), the EuclidEmulator (Euclid Collaboration: Knabenhans et al. 2019), the BACCO emulator (Angulo et al. 2021) or the Mira Titan emulator (Heitmann et al. 2016). Predictions for the γ-2PCFs are finally computed from Eq. (1) as:

$$\xi_\pm^{ij}(\vartheta) = \frac{1}{2\pi}\int_0^\infty C_\ell^{ij}\,J_{0/4}(\ell\vartheta)\,\ell\,\mathrm{d}\ell, \qquad (3)$$

where $J_{0/4}(x)$ are Bessel functions of the first kind. In this paper, these calculations are carried out by pyccl[2] (Chisari et al. 2019). The $n^i(z)$ are taken from the LSST Science Requirement Document (The LSST Dark Energy Science Collaboration et al. 2018) and given by

$$n(z) = N_0 z^2 \exp\left[-\left(\frac{z}{z_0}\right)^\alpha\right], \qquad (4)$$

with $(z_0,\alpha) = (0.13, 0.78)$ and N_0 normalised to provide a number density of $n_{\rm eff} = 3.0$ gal arcmin^{-2}. This lower than the expected number density for the first data release ($n_{\rm eff} = 10$ gal arcmin^{-2}), but is large enough to validate the methods presented in this paper and makes the calculation more tractable. The $n(z)$ is further split into five equi-populated tomographic bins, and smoothed with a Gaussian filter of width $\sigma = 0.05(1+z)$ in order to mimic the photometric selection process [*confirm with Niko*]. The resulting distributions[3] are shown in Figure 1.

⋆ E-mail: joachim.harnois-deraps@ncl.ac.uk
[1] See Kilbinger et al. (2017) for a comparison between the Limber approximation and the exact calculations.

[2] pyccl:pypi.org/project/pyccl
[3] The construction of these tomographic $n(z)$ can be reproduced in github...CCL_SRD_Niko.

The cosmic shear signal can be measured from the ellipticities $\epsilon_{1/2}$ of simulated or observed galaxies, which, in absence of systematics and secondary signals, are unbiased estimators of the cosmic shear components $\gamma_{1/2}$. The γ-2PCF are then estimated as:

$$\widehat{\xi}^{ij}_{\pm}(\vartheta) = \frac{\sum_{a,b} w_a w_b \left[\epsilon^i_{a,\mathrm{t}}\epsilon^j_{b,\mathrm{t}} \pm \epsilon^i_{a,\times}\epsilon^j_{b,\times}\right]\Delta_{ab}(\vartheta)}{\sum_{a,b} w_a w_b}\,, \tag{5}$$

where the sum is over all pairs of galaxies a, b separated by an angular separation ϑ, taken from tomographic bins i, j. The tangential/cross components of their ellipticities are denoted as $\epsilon_{\mathrm{t}/\times}$, respectively. $\Delta_{ab}(\vartheta)$ is the binning operator, equal to unity if the angular separation between the two galaxies falls within the ϑ-bin, and zero otherwise, and the shape weights $w_{a,b}$ are set to unity. The measurements are carried out by TREECORR (Jarvis et al. 2004), in which we set the BIN_SLOP parameter to 0.05. We compute the correlations in nine logarithmically-spaced angular bins ranging from 0.5 to 475.5 arcmin.

We produce convergence maps from each of these catalogues by assigning the shear signal onto spherical HEALPIX[4] maps (Górski et al. 2005) with $N_{\mathrm{side}} = 4096$, then using the standard Kaiser & Squires inversion technique (Kaiser & Squires 1993) implemented in HEALPY to reconstruct a convergence maps with the same angular resolution, including a 2.0 arcmin smoothing beam in the inverse transform.

[*Some of this should go in the simulation section]*

2.2 Beyond-2pt

Mention the different probes, how they are measured, some on galaxy catalogues, some on kappa maps... Kappa: Peaks, minima, lensing PDF, Map3, Map2, MF, shear cats: squeezed bispectrum, DSS, three-point... models: lensing PDF, squeezed bispectrum, Map2, Map3, DSS

3 INTRINSIC ALIGNMENT MODELS

Galaxies interact with the tidal forces caused by the large-scale structure they live in, causing their intrinsic shapes to acquire correlated alignments that has nothing to do with the correlations caused by weak lensing. This therefore acts as a secondary signal that contaminates the shape correlation measurements carried out in a cosmic shear analysis. There is no consensus on the actual physical model that describes the IA signal, and even when adopting these, the free parameters they contain are only weakly constrained from the data (see **?**, for a review). In this paper we consider four such IA models that we describe in the following sub-sections. In all cases, our models couple the galaxy intrinsic shapes with the local over-density and projected tidal field , then prescribe an intrinsic ellipticity tensor $\gamma^{\mathrm{IA}}_{ij}$, from which observed ellipticities are extracted as:

$$\epsilon^{\mathrm{IA}}_1 = \gamma^{\mathrm{IA}}_{xx} - \gamma^{\mathrm{IA}}_{yy}\,, \qquad \epsilon^{\mathrm{IA}}_2 = 2\gamma^{\mathrm{IA}}_{xy}\,. \tag{6}$$

3.1 Non-linear alignment (NLA)

The NLA model of Bridle & King (2007) is the most widely used IA model in the cosmic shear literature thus far. According to the NLA, IA are caused by a linear coupling between galaxy shapes and the non-linear large-scale tidal field at the galaxy position. In the context of two-point functions, these intrinsic shapes contribute to an intrinsic-intrinsic (*II*) term and an intrinsic-shear coupling (*GI*) term (Hirata & Seljak 2004), both secondary signals to the true cosmic shear (*GG*) term, with the latter typically dominating the IA sector in cross-tomographic measurements. The *II* and *GI* terms can be both computed from the matter power spectrum as:

$$P_{II}(k,z) = \left(\frac{A_{\mathrm{IA}}\bar{C}_1\bar{\rho}(z)}{D(z)}\right)^2 a^4(z)P_\delta(k,z) \tag{7}$$

and

$$P_{GI}(k,z) = -\frac{A_{\mathrm{IA}}\bar{C}_1\bar{\rho}(z)}{D(z)}a^2(z)P_\delta(k,z)\,, \tag{8}$$

which can then be past to the Limber integration (Eqs. 1 and 3) to compute the secondary signals $\xi^{II}_\pm(\vartheta)$ and $\xi^{GI}_\pm(\vartheta)$. In the above expression, $D(z)$ is the linear growth factor, $\bar{\rho}(z)$ is the mean matter density at redshift z and $\bar{C}_1 = 5\times10^{-14}M^{-1}_\odot h^{-2}\mathrm{Mpc}^3$ is a constant calibrated in Brown et al. (2002). The strength of the tidal coupling is modulated by the amplitude parameter A_{IA}, which is the main NLA parameter constrained by current cosmic shear surveys. Note that this model can be augmented by redshift and luminosity dependences, however we do not use these here.

The NLA intrinsic ellipticities $\epsilon^{\mathrm{NLA}}_{1,2}$ are related to tidal field s_{ij} by:

$$\epsilon^{\mathrm{NLA}}_1 = -\frac{A_{\mathrm{IA}}\bar{C}_1\bar{\rho}(z)}{D(z)}(s_{xx}-s_{yy}) \;\;, \epsilon^{\mathrm{NLA}}_2 = -\frac{2A_{\mathrm{IA}}\bar{C}_1\bar{\rho}(z)}{D(z)}s_{xy}\,, \tag{9}$$

where $s_{ij} = \partial_{ij}\phi$ are the Cartesian components of the tidal tensor of the gravitational potential. Note that the term 'non-linear' in the model name can be misleading, as it refers to the non-linear matter power spectrum $P(k)$ that is used in its calculations; the coupling between the intrinsic galaxy shapes and the tidal field is still linear. Eq.(9) is used to assign intrinsic ellipticities to galaxies, given maps of the tidal field components s_{xx}, s_{yy} and s_{xy} (see Sec. 4.3).

3.2 δ-NLA

The NLA model presented in the last section has been widely used in cosmic data analyses, but it has important known limitations and is therefore bound to fail at describing the IA signal with high precision. A perturbation theory extension to the NLA has been introduced in Blazek et al. (2015) and Blazek et al. (2019), where it is recognised that higher order couplings could be important and should be considered. The first additional term to be included is the over-density weighting term, which is caused by the fact that the intrinsic alignment of galaxies can only be observed at the galaxy positions, which are not distributed randomly on the sky but instead trace the underlying matter density, 'δ', although the exact biasing scheme is not currently know. Accounting for this extra term in theoretical predictions is done with one-loop perturbation theory (Blazek et al. 2019), and is implemented in PYCCL. Physically, it corresponds to adding a δ-weight to the NLA predictions at the local galaxy positions, effectively representing the different tracer properties. At the level of numerical simulations, this could be done in principle simply by augmenting the NLA ellipticities with this weight, namely:

$$\epsilon^{\delta-\mathrm{NLA}}_{1/2} = \epsilon^{\mathrm{NLA}}_{1/2} \times (1 + b_{\mathrm{TA}}\delta)\,, \tag{10}$$

where the term b_{TA} corresponds to the (largely unconstrained) biasing relation between these source galaxies and the underlying matter field. In practice, however, we find that this is noisy, and that it is instead preferable to generate mocks catalogues with the biasing scheme directly applied when assigning galaxy positions, after which no weighting is necessary. Nevertheless, Eq. (10) can be used

[4] HEALPIX: http://healpix.sf.net

to modify the value of $b_{\rm TA}$. Indeed, from a mock with a given bias $b_{\rm TA,orig}$, we can rescale the IA contribution to a different $b_{\rm TA,new}$ as:

$$\boldsymbol{\epsilon}^{\rm int}_{b_{\rm TA,new}} = \frac{(1 + b_{\rm TA,new}\delta)}{(1 + b_{\rm TA,orig}\delta)} \boldsymbol{\epsilon}^{\rm int}_{b_{\rm TA,orig}} \,. \tag{11}$$

Compared to the NLA, the δ-NLA is a stronger IA model, especially on small scales (Blazek et al. 2019), and seems to be preferred by some hydrodynamical simulations (Hilbert et al. 2017). It is also better motivated from a physical point of view, since we know that the galaxies trace dark matter and are not randomly distributed in our Universe as the NLA assumes.

3.3 Tidal Torque (TT)

As shown in Blazek et al. (2019), one-loop perturbative calculations include another term, by which galaxies acquire an intrinsic alignment via a coupling between their angular momentum and the tidal field, which can be re-expressed as a quadratic coupling between the tidal field and the shape. In this tidal torque model (TT), intrinsic ellipticities are given by:

$$\gamma^{\rm IA,TT}_{ij} = C_2 \left[\sum_{k=x,y,z} s_{ik} s_{kj} - \frac{1}{3}\delta_{ij} s^2 \right] , \tag{12}$$

where

$$C_2 = \frac{5A_2 \bar{C}_1 \Omega_{\rm m} \rho_{\rm crit}}{D^2(z)} = \left[\frac{-5A_2}{A_1 D(z)} \right] C_1 . \tag{13}$$

Under the approximation that line-of-sight alignments are mostly suppressed from cosmic shear measurement due to the broad lensing kernels, we show in Appendix A that the terms inside the square bracket in Eq. (12) leads to:

$$\epsilon^{\rm TT}_1 = C_2 \left[s^2_{xx} - s^2_{yy} \right] , \epsilon^{\rm TT}_2 = 2C_2 s_{xy} \left[s_{xx} + s_{yy} \right] , \tag{14}$$

both quadratic in the tidal field components.

3.4 δ-TT

Following the relation between the NLA and the δ-NLA model, galaxies in the TT model are also assume to be randomly scattered on the sky, which we know to be a bad approximation. Computing the next-order contribution to the TT model involves two-loop perturbation theory calculations that have not been done yet due to the significantly higher complexity of such task. in simulations however, the δ-weighting term is straight-forward to implement, as it involves to simply infuse the TT model onto galaxies that trace the matter field with a non-zero biasing factor. As for the δ-NLA model, the δ-TT ellipticities can be related to the TT model as:

$$\epsilon^{\delta-{\rm TT}}_{1/2} = \epsilon^{\rm TT}_{1/2} \times (1 + b_{\rm TA}\delta) \,. \tag{15}$$

There are currently no theoretical models for δ-TT, which means that predictions from this model are, at the moment, completely simulation-based.

It is worth recalling here that other IA models exist in the literature, and that at this point observations are not precise enough to set strong constraints on them, further motivating our flexible multi-model approach.

4 SIMULATIONS

4.1 Cosmic shear galaxy catalogues

The weak lensing simulations developed for this work are based on ray-tracing mass sheets produced from the Outer Rim N-body simulation (Heitmann et al. 2019), which evolved $10{,}240^3$ particles in a $(5.225\ {\rm Gpc})^3$ cosmological volume, assuming a flat ΛCDM cosmology with $\Omega_{\rm m}$=0.2648, $\Omega_{\rm b}$=0.0448, h=0.71, σ_8 = 0.801, $n_{\rm s}$= 0.963, w_0=-1.00. A total of 101 particle snapshots were originally saved, of which we use only those with $z < 4.0$. Particles from each dump are assigned to curved mass shells approximately 114 Mpc thick, producing a sequence of 57 HEALPIX maps $\delta(\theta, \phi, \chi_i)$ with NSIDE = 8192 and i = 1..57, filling up a light-cone over an octant up to z = 3.

Ray-tracing is performed in the Born approximation, summing over the mass shells using the χ-integral of Eq. (1). A source plane is placed at the high-redshift edge of every mass planes, resulting in a series of convergence maps $\kappa(\theta, \phi, \chi_i)$ that are subsequently transformed into shear maps $\gamma_{1/2}(\theta, \phi, \chi_i)$ using the Kaiser-Squires methods (Kaiser & Squires 1993), which is implemented via efficient HEALPY ALM2MAP routines.

We position galaxies in the light cone following exactly our chosen $N(z)$, and interpolate the shear quantities at their location. We follow two distinct algorithm to achieve this:

(i) *Random:* galaxies RA and Dec are distributed randomly on the octant, thereby matching this fundamental assumptions in the NLA and TT models.

(ii) *Linear bias:* galaxies RA and Dec are sampled from the mass sheets smoothed[5] over 1.0 h^{-1}Mpc (comoving), assuming a linear bias of $b_{\rm TA}$, now matching instead the assumptions of the δ-NLA and δ-TT models. With this method we produce galaxy positions assuming first $b_{\rm TA}$ = 1.0 (our fiducial case) and also $b_{\rm TA}$ = 2.0, enhancing the model flexibility.

Since source clustering is a higher order effect in cosmic shear, the measured $\xi_\pm$ from these three mocks (random, $b_{\rm TA}$ = 1.0 and $b_{\rm TA}$ = 2.0) show negligible differences (*to quantify and cite*). In contrast, the impact on the IA contamination is significant and can double the secondary signal in certain circumstances. The main explanation for this is that while clustered sources are uncorrelated with the foreground matter responsible for the lensing signal, the high-density regions they live are also subject to the largest tidal fields.

4.2 Projected tidal fields

Our infusion method completely relies on couplings between intrinsic galaxy shapes and the local tidal field, hence the first step in our method consist in extracting the tidal field maps $s_{ij}(\theta, \phi, \chi_i)$ from the mass maps $\delta(\theta, \phi, \chi_i)$ that source them. In three dimensions, trace-free tidal tensor $s_{ij}(\boldsymbol{x})$ can be obtained from the matter over-density field $\delta(\boldsymbol{x})$ as (Catelan et al. 2001):

$$\widetilde{s}_{ij}(\boldsymbol{k}) = \left[\frac{k_i k_j}{k^2} - \frac{\delta_{ij}}{3} \right] \widetilde{\delta}(\boldsymbol{k}) \mathcal{G}(\sigma_{\rm G}) \,, \tag{16}$$

where $\mathcal{G}(\sigma_{\rm G})$ is a three-dimensional Gaussian function described by a single (free) parameter $\sigma_{\rm G}$ that controls the physical scales which are allowed to affect the IA term in our model. Tilde symbols denote Fourier transformed quantities, the indices (i, j) label the components of the Cartesian wave-vector $\boldsymbol{k}^T = (k_x, k_y, k_z)$, and

[5] We also tried sampling the field with 0.1 and 0.5 h^{-1}Mpc but this resulted in noisier results.

Figure 2. Density field and the associated projected tidal field tensors.

$k^2 = k_x^2 + k_y^2 + k_z^2$. As shown in Harnois-Déraps et al. (2021) for Cartesian coordinates, projected tidal fields computed from projected mass sheets provide and excellent agreement with the NLA model, which in contrast computes the full tidal fields from the three-dimensional matter density and project along the radial dimension at the end. We promote this transformation to curved-sky in this work, exploiting the polarisation ALM2MAP operations built in HEALPY. In particular, noting that $Q = s_{xx} - s_{yy}$, $U = s_{xy}$ and $\delta = s_{xx} + s_{yy}$, we compute the curved-sky tidal field tensors $s_{ij}(\boldsymbol{\theta})$ as:

$$s_{xx}(\boldsymbol{\theta}) = \left[\frac{\delta + Q}{2} - \frac{\delta}{3}\right], s_{yy}(\boldsymbol{\theta}) = \left[\frac{\delta - Q}{2} - \frac{\delta}{3}\right], s_{xy}(\boldsymbol{\theta}) = U \qquad (17)$$

where the $U(\boldsymbol{\theta})$ and $Q(\boldsymbol{\theta})$ maps are smoothed by the Gaussian beam with width $\sigma_{\rm G}$. We suppress large artificial tidal fields at the maps boundary by replicating 8× the density maps defined on the octant and working on a full sky density δ; we re-apply the octant mask on the tidal field maps after the operation. Note that the value of $\sigma_{\rm G}$ is a free parameter both in the infusion technique described in this paper and in the NLA and TATT models. We therefore explore two cases, $\sigma_{\rm G} = 0.1$Mpc and 0.5Mpc, however this may be further optimised in the future.

Projected tidal field maps s_{11}, s_{22} and s_{12} are constructed that way for each mass sheets; Fig. 2 shows the three tidal fields and the mass maps for one of them. We can clearly see the connection between all maps around over-dense regions. *(Include a figure of $s_i j$ and δ).*

[Mention normalisation of the tidal fields by $0.6252 = H_0/114$ *= 1/shell-thickness*

4.3 Infusion of intrinsic alignments

Having now produced shear catalogues and tidal field maps, we can now use Eq. 9 to couple linearly the alignment of galaxies with the local tidal field, or Eq. 12 to use instead a quadratic coupling. These allow us to compute the intrinsic ellipticities $\boldsymbol{\epsilon}^{\rm int}$ for the four IA models described in Sec. 3, which we combine with the cosmic shear signal $\boldsymbol{g}$ to compute observed ellipticities:

$$\boldsymbol{\epsilon}^{\rm obs} = \frac{\boldsymbol{\epsilon}^{\rm int} + \boldsymbol{g}}{1 + \boldsymbol{\epsilon}^{\rm int}\boldsymbol{g}^*}, \text{with } \boldsymbol{\epsilon}^{\rm int} = \frac{\boldsymbol{\epsilon}^{\rm IA} + \boldsymbol{\epsilon}^{\rm ran}}{1 + \boldsymbol{\epsilon}^{\rm IA}\boldsymbol{\epsilon}^{\rm ran,*}}. \qquad (18)$$

In the above expressions, the denominators ensures that the combined ellipticities never exceed unity. The complex spin-2 reduced shear $\boldsymbol{g} \equiv (\gamma_1 + {\rm i}\gamma_2)/(1+\kappa)$ is computed from the shear ($\gamma_{1/2}$) and convergence (κ) maps, interpolated at the galaxy positions and redshifts. The random orientation term $\boldsymbol{\epsilon}^{\rm ran}$ is drawn from two Gaussians (one per component) with their standard deviations matching the LSST-Y1 forecast, $\sigma_\epsilon = 027$. We further constraint the random ellipticity to satisfy $|\boldsymbol{\epsilon}^{\rm ran}| \leqslant 1.0$. We re-iterate here that the same tidal fields, shear maps and IA coupling equations are used for the NLA and δ-NLA models, and separately for the TT and δ-TT models; these only differ by the fact that in one case the galaxies are placed at random on the octant, while in the other case they are linearly tracing the dark matter.

Also note that our current IA models make no differentiation between galaxy colours or type, and instead treats the full sample as a single population that has a single, effective, alignment signall (see Samuroff et al. 2019, for an example with a red/blue split).

model	$(A_{\rm IA}, b_{\rm TA}, A_2)$
NLA	(±1,0,0)
δ−NLA	(±1,1,0)
	(1,2,0)
TT	(0,0,±1)
δ-TT	(0,1,±1)
	(0,2,1)
TATT- fiducial	(1,1,1)

Table 1. IA models infused in this work.

5 VALIDATION WITH $\xi_\pm$

5.1 NLA model

See Fig. 3

5.2 δ-NLA model

See Fig. 4.

We verified that it works equally well for $b_{\rm TA} = 1.0$ and 2.0.

Using this, we $b_{\rm TA}$-rescale our $b_{\rm TA} = 1.0$ mock to $b_{\rm TA} = 2.0$ and to 0.0 mocks. Results are shown in Fig. 5 for one of the tomographic bin. It works reasonably well, but lower redshift are less accurate due to the increased shot noise (not shown), hence we do not recommend using this.

5.3 TT model

See Fig. 6

To match the theory, we need to apply the following calibration: $\epsilon^{\rm IA,TT}(z < 0.5) \rightarrow \epsilon^{\rm IA,TT}/2.5$.

5.4 δ-TT model

See Fig. 7

To match the TT theory, we need to apply the following calibration: $\epsilon^{\rm IA,TT}(z < 0.5) \rightarrow \epsilon^{\rm IA,TT}/5.0$, followed by $\epsilon^{\rm IA,TT} \rightarrow \epsilon^{\rm IA,TT}/7.0$.

6 HIGHER-ORDER WEAK LENSING STATISTICS

... use the mocks from Table 1 to compute derivatives. Show.

7 CONCLUSIONS

ACKNOWLEDGEMENTS

JHD acknowledges support from an STFC Ernest Rutherford Fellowship (project reference ST/S004858/1). Ray-tracing computations were carried on the NERSC [acknowledgments] ... HACC [acknowledgements] ... OuterRim [Acknowledgments]

Some of the results in this paper have been derived using the HEALPY and HEALPIX packages.

All authors contributed to the development and writing of this paper. JHD led the analysis....

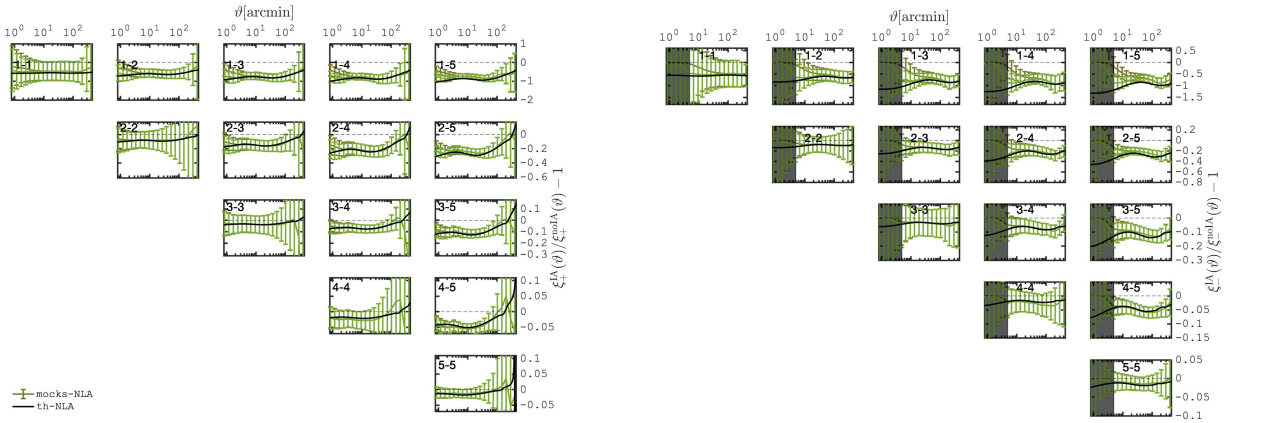

Figure 3. Ratio between the shear correlation functions with and without IA, assuming the NLA model with $A_{\rm IA} = 1.0$ both in the simulations and theory. Measurements shown in green and brown correspond to smoothing scales of 0.1 and 0.5 h^{-1}Mpc in the tidal field. There is no shape noise in the simulations, but it is included in the error bars.

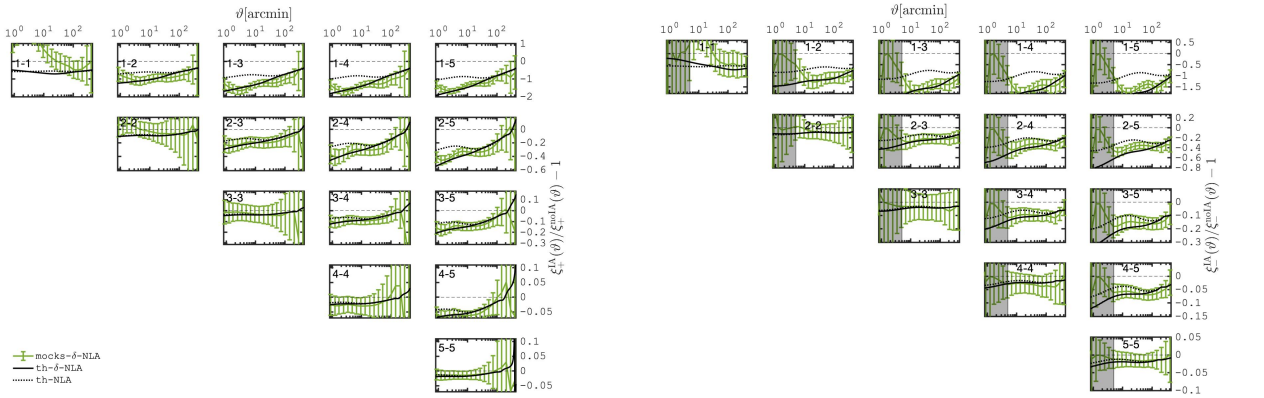

Figure 4. Same as Fig. 3, but for the δ-NLA model with $A_{\rm IA} = 1.0$ and $b_{\rm TA} = 1.0$, and only for smoothing of $0.5h^{-1}$Mpc. The dashed black lines show the NLA predictions to better highlight the differences.

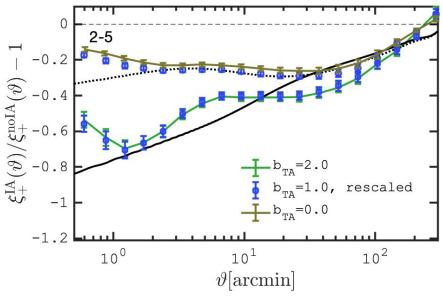

Figure 5. Ratio between the shear correlation functions with and without IA in tomographic bin combination 2-5. The brown and green symbols show measurements from simulations constructed with $b_{\rm TA} = 0.0$ and 2.0 respectively, the black solid and dotted lines shown their predictions, while the blue symbols are obtained by rescaling $b_{\rm TA} = 1.0$ simulations using Eq. 11.

DATA AVAILABILITY

REFERENCES

Angulo, R. E., Zennaro, M., Contreras, S., Aricò, G., Pellejero-Ibañez, M., & Stücker, J. 2021, MNRAS, 507, 5869, 2004.06245

Blazek, J., Vlah, Z., & Seljak, U. 2015, JCAP, 2015, 015, 1504.02510

Blazek, J. A., MacCrann, N., Troxel, M. A., & Fang, X. 2019, Phys. Rev. D, 100, 103506, 1708.09247

Bridle, S., & King, L. 2007, New Journal of Physics, 9, 444, 0705.0166

Brown, M. L., Taylor, A. N., Hambly, N. C., & Dye, S. 2002, MNRAS, 333, 501, astro-ph/0009499

Catelan, P., Kamionkowski, M., & Blandford, R. D. 2001, MNRAS, 320, L7, astro-ph/0005470

Chisari, N. E. et al. 2019, ApJS, 242, 2, 1812.05995

Euclid Collaboration: Knabenhans, M. et al. 2019, MNRAS, 484, 5509, 1809.04695

Górski, K. M., Hivon, E., Banday, A. J., Wandelt, B. D., Hansen, F. K., Reinecke, M., & Bartelmann, M. 2005, ApJ, 622, 759, arXiv:astro-ph/0409513

Harnois-Déraps, J., Martinet, N., & Reischke, R. 2021, MNRAS, 2107.08041

Heitmann, K. et al. 2016, ApJ, 820, 108

——. 2019, ApJS, 245, 16, 1904.11970

Hilbert, S., Xu, D., Schneider, P., Springel, V., Vogelsberger, M., & Hernquist, L. 2017, MNRAS, 468, 790, 1606.03216

Hirata, C. M., & Seljak, U. 2004, Phys. Rev. D, 70, 063526, astro-

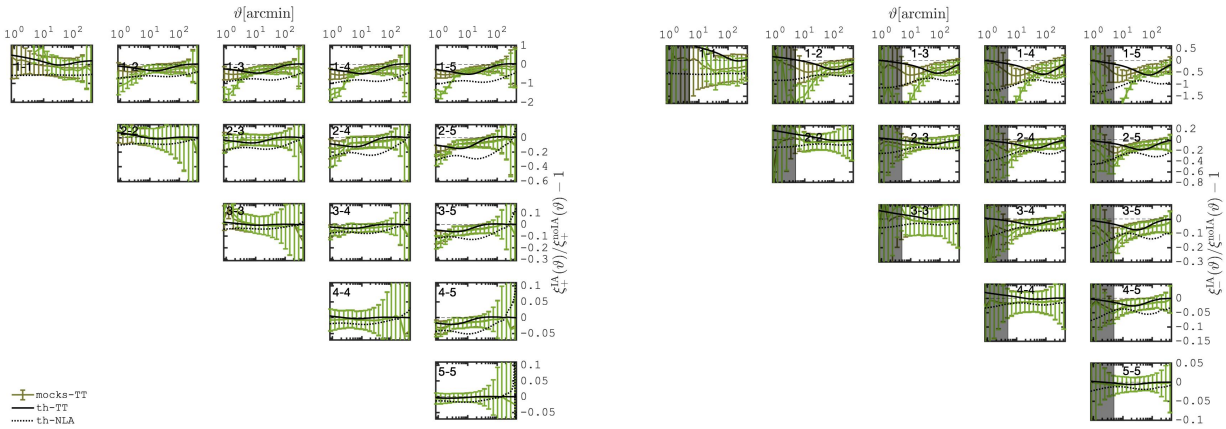

Figure 6. Same as Fig. 3, but for the TT model with $A_2 = 1.0$. Here, the dashed black lines show the NLA predictions to better highlight the differences.

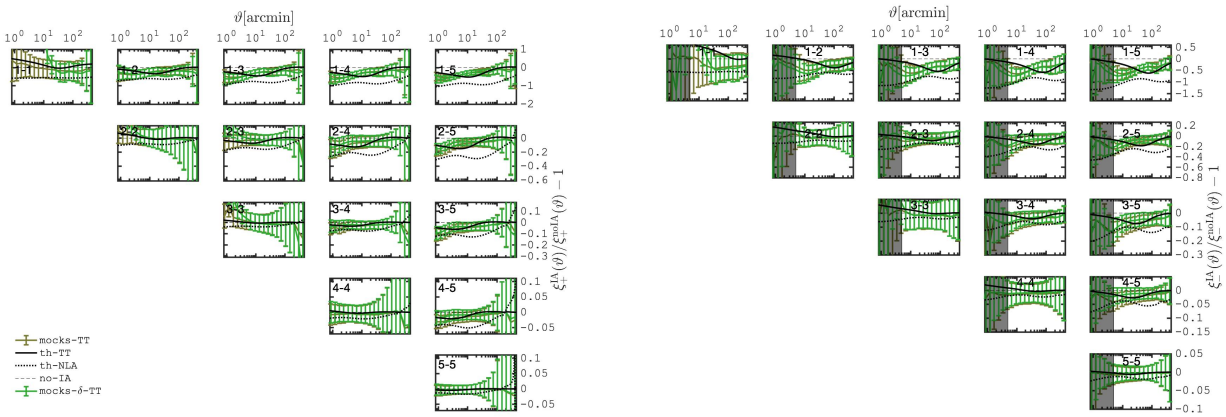

Figure 7. Same as Fig. 4, but comparing the TT and the δ-TT models, with $A_2 = 1.0$, $b_{\rm TA} = 1.0$, and only for smoothing of $0.5h^{-1}$Mpc.

ph/0406275
Jarvis, M., Bernstein, G., & Jain, B. 2004, MNRAS, 352, 338
Kaiser, N., & Squires, G. 1993, ApJ, 404, 441
Kilbinger, M. et al. 2017, MNRAS, 472, 2126, 1702.05301
Mead, A., Brieden, S., Tröster, T., & Heymans, C. 2020, arXiv e-prints, arXiv:2009.01858, 2009.01858
Samuroff, S. et al. 2019, MNRAS, 489, 5453, 1811.06989
Takahashi, R., Sato, M., Nishimichi, T., Taruya, A., & Oguri, M. 2012, ApJ, 761, 152
The LSST Dark Energy Science Collaboration et al. 2018, arXiv e-prints, arXiv:1809.01669, 1809.01669

APPENDIX A: PROJECTED TIDAL FIELD

[To reword] We derive in this Appendix... The prescription to assign an intrinsic alignment based on the projected tidal field, described in Eq. (9), involves the combinations $(s_{xx} - s_{yy})$ and s_{xy}, which therefore correspond to:

$$\widetilde{\epsilon}_1^{\rm IA}(\boldsymbol{k}_\perp) \propto \left(\frac{k_x^2 - k_y^2}{k^2}\right)\widetilde{\delta}_{\rm 2D}(\boldsymbol{k}_\perp)\mathcal{G}_{\rm 2D}(\sigma_{\rm G}),$$
$$\widetilde{\epsilon}_2^{\rm IA}(\boldsymbol{k}_\perp) \propto \left(\frac{k_x k_y}{k^2}\right)\widetilde{\delta}_{\rm 2D}(\boldsymbol{k}_\perp)\mathcal{G}_{\rm 2D}(\sigma_{\rm G}) \qquad \text{(A1)}$$

Aside from the smoothing kernel, these are the same filters that are used for converting convergence maps to shear maps under the Kaiser & Squires (1993, KS hereafter) inversion:

$$\widetilde{\gamma}_1(\boldsymbol{\ell}) = \left(\frac{k_x^2 - k_y^2}{k^2}\right)\widetilde{\kappa}(\boldsymbol{\ell}), \qquad \widetilde{\gamma}_2(\boldsymbol{\ell}) = \left(\frac{k_x k_y}{k^2}\right)\widetilde{\kappa}(\boldsymbol{\ell}) \qquad \text{(A2)}$$

meaning that on can linearly combine the mass sheets with the correct coefficients and obtain intrinsic ellipticities from a normal KS inversion.

Projecting out the z components (e.i. s_{0i}=s_{i0}=0 for all i), the tidal torque terms from Eq. (12) can be expanded as:

$$\gamma_{ij}^{\rm TT} = C_2\left[\sum_{k=x,y} s_{ik}s_{kj} - \frac{1}{3}\delta_{ij}s^2\right] \qquad \text{(A3)}$$
$$= C_2\left[s_{ix}s_{xj} + s_{iy}s_{yj} - \frac{1}{3}\delta_{ij}\left(s_{xx}^2 + s_{yy}^2 + 2s_{xy}^2\right)\right]. \qquad \text{(A4)}$$

Specifically, this yields:

$$\gamma_{xx}^{\rm TT} = C_2\left[\frac{2}{3}s_{xx}^2 - \frac{1}{3}s_{yy}^2 + \frac{1}{3}s_{xy}^2\right],$$
$$\gamma_{yy}^{\rm TT} = C_2\left[-\frac{1}{3}s_{xx}^2 + \frac{2}{3}s_{yy}^2 + \frac{1}{3}s_{xy}^2\right], \qquad \text{(A5)}$$
$$\gamma_{xy}^{\rm TT} = C_2 s_{xy}\left[s_{xx} + s_{yy}\right].$$

With the standard ellipticity definitions $\epsilon_1^{\rm TT} \equiv \gamma_{xx}^{\rm TT} - \gamma_{yy}^{\rm TT}$ and $\epsilon_2^{\rm TT} \equiv -2\gamma_{xy}$, we obtain:

$$\epsilon_1^{\rm TT} = C_2 \left[s_{xx}^2 - s_{yy}^2 \right], \epsilon_2^{\rm TT} = -2C_2 s_{xy} \left[s_{xx} + s_{yy} \right]. \quad \text{(A6)}$$

In the TATT model, the total intrinsic ellipticity component is therefore given by $\epsilon_{1/2}^{\rm IA} = \epsilon_{1/2}^{\rm TATT} = \epsilon_{1/2}^{\delta-{\rm NLA}} + \epsilon_{1/2}^{\rm TT}$.

This paper has been typeset from a TEX/ LATEX file prepared by the author.